FULL PAPER

5th Anniversary Article

ADVANCED
SCIENCE
Open Access

www.advancedscience.com

A Lesson from Plants: High-Speed Soft Robotic Actuators

*Richard Baumgartner, Alexander Kogler, Josef M. Stadlbauer, Choon Chiang Foo,
Rainer Kaltseis, Melanie Baumgartner, Guoyong Mao, Christoph Keplinger,
Soo Jin Adrian Koh, Nikita Arnold, Zhigang Suo, Martin Kaltenbrunner,*
and Siegfried Bauer*

This publication is dedicated to Siegfried Bauer, who has sadly passed away during the course of this work

Rapid energy-efficient movements are one of nature's greatest developments. Mechanisms like snap-buckling allow plants like the Venus flytrap to close the terminal lobes of their leaves at barely perceptible speed. Here, a soft balloon actuator is presented, which is inspired by such mechanical instabilities and creates safe, giant, and fast deformations. The basic design comprises two inflated elastomer membranes pneumatically coupled by a pressurized chamber of suitable volume. The high-speed actuation of a rubber balloon in a state close to the verge of mechanical instability is remotely triggered by a voltage-controlled dielectric elastomer membrane. This method spatially separates electrically active and passive parts, and thereby averts electrical breakdown resulting from the drastic thinning of an electroactive membrane during large expansion. Bistable operation with small and large volumes of the rubber balloon is demonstrated, achieving large volume changes of 1398% and a high-speed area change rate of 2600 cm^2 s^{-1}. The presented combination of fast response time with large deformation and safe handling are central aspects for a new generation of soft bio-inspired robots and can help pave the way for applications ranging from haptic displays to soft grippers and high-speed sorting machines.

1. Introduction

Nature inspires artificial systems, particularly regarding motion. Quick and large movements are keenly sought-after for applications in rigid and soft robotics, industrial automation, and modern prosthetics.[1–5] In recent years, the development of artificial muscles that mimic the basic function of human and animal musculature has gained an importance due to its wide range of potential applications.[6] But there are examples in which direct muscle action alone cannot be responsible for the rapid movement. The jaw muscles of hummingbirds are not strong enough to close the beak in the observed short amount of time. However, hummingbirds are able to bend their lower jaw and use a controlled elastic instability to rapidly snap it from the open to the closed position.[7] Completely without muscle

Dr. R. Baumgartner, Dr. A. Kogler, J. M. Stadlbauer, Dr. R. Kaltseis,
M. Baumgartner, Prof. M. Kaltenbrunner, Prof. S. Bauer[†]
Soft Matter Physics
Institute of Experimental Physics
Johannes Kepler University Linz
Altenberger Straße 69, 4040 Linz, Austria
E-mail: martin.kaltenbrunner@jku.at

J. M. Stadlbauer, M. Baumgartner, Dr. G. Mao, Dr. N. Arnold,
Prof. M. Kaltenbrunner
Soft Materials Lab
Linz Institute of Technology LIT
Johannes Kepler University Linz
Altenberger Straße 69, 4040 Linz, Austria

[†]Deceased December 2018.

Dr. C. C. Foo
Institute of High Performance Computing
A*STAR
1 Fusionopolis Way, #16-16 Connexis, Singapore 138632, Singapore

M. Baumgartner
Institute of Polymer Science
Johannes Kepler University Linz
Altenberger Straße 69, 4040 Linz, Austria

Prof. C. Keplinger
Department of Mechanical Engineering
University of Colorado Boulder
Boulder, CO 80309, USA

Prof. C. Keplinger
Materials Science and Engineering Program
University of Colorado Boulder
Boulder, CO 80303, USA

Prof. S. J. A. Koh
Department of Mechanical Engineering
National University of Singapore
Singapore 117575, Singapore

Prof. Z. Suo
John A Paulson School of Engineering and Applied Sciences
Harvard University
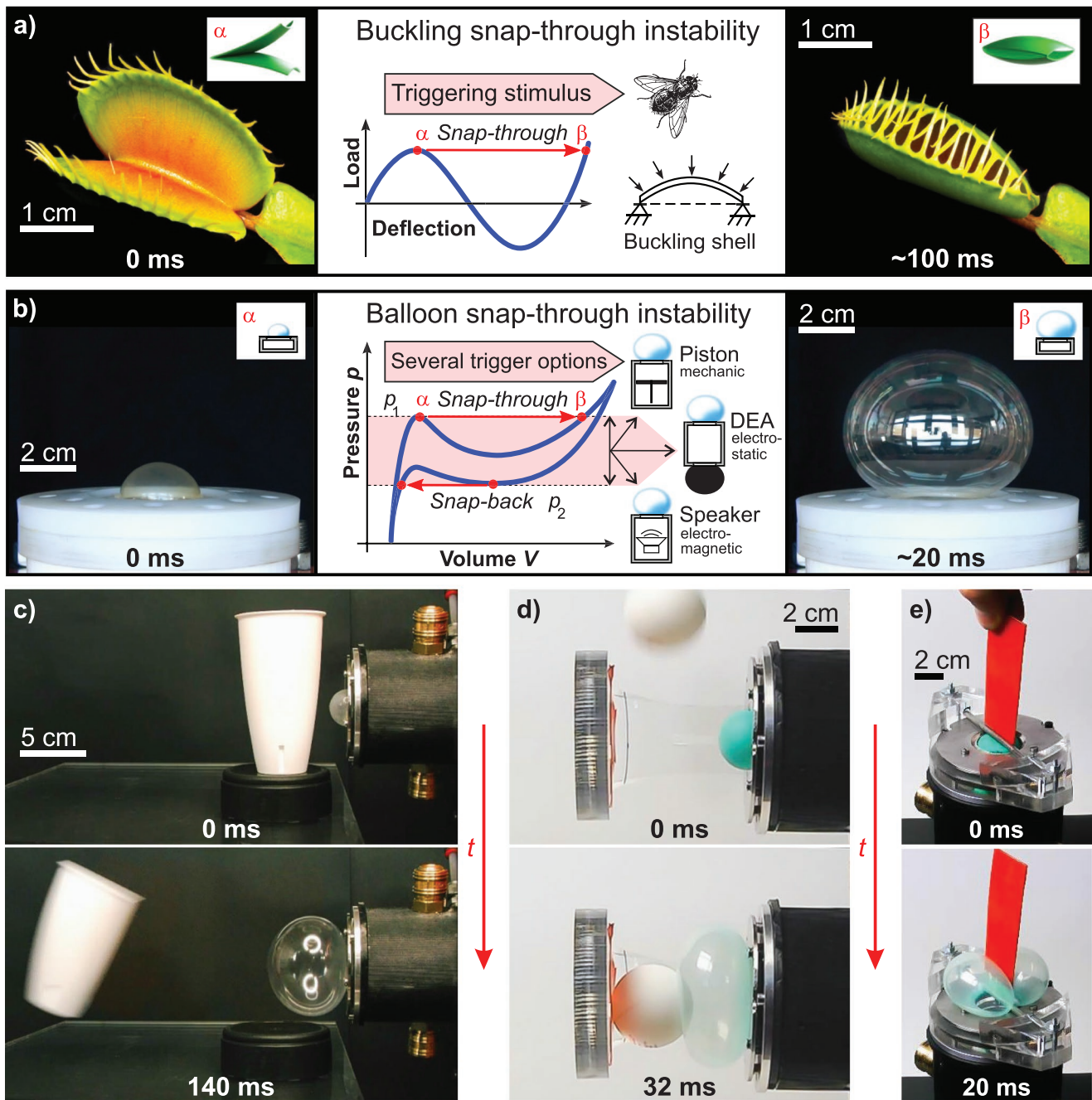29 Oxford Street, Cambridge, MA 02138, USA

Figure 1. Harnessing mechanical instability to improve the speed of actuation. a) The Venus flytrap uses a stimulus-triggered mechanical buckling instability. b) Mechanical balloon snap-through instability enables high-speed actuation. Characteristic pressure–volume behavior of a rubber membrane: As soon as the pressure reaches the critical pressures p_1 or p_2, a further insignificant pressure increase or decrease rapidly changes the membrane volume in just a few milliseconds. Under pressure-controlled conditions, snap-through instability can be triggered by different kinds of pressure sources. c) Possible application as fast sorting device, e.g., for conveyor belts; d) fast and soft gripper catching a ping-pong ball; e) handling of sensitive objects by improving compliance with additional constraints (Video S1, Supporting Information).

support, plants rely solely on mechanical instabilities for rapid movement. The inherent motility of plants is the consequence of selective swelling and shrinking caused by water flow driven by osmosis and evaporation phenomena.[8] These processes are rather slow and therefore limit the overall speed. Plants like the Venus flytrap can overcome this limit by suddenly releasing stored elastic energy resulting in one of the fastest movements

($\approx$100 ms) in the plant world.[9,10] The rapid closure of the Venus flytrap is made possible by harnessing a snap-buckling instability (**Figure 1**a). Due to geometric constraint and elastic properties of the doubly curved terminal lobes which form the trap at the tip of each leaf the plant can accumulate elastic energy and release it if triggered by an external stimulus.[9,11] Here, we took a lesson from plants and transferred the idea of

**ADVANCED
SCIENCE NEWS**

www.advancedsciencenews.com

**ADVANCED
SCIENCE**
Open Access

www.advancedscience.com

how mechanical instabilities are key to the rapid actuation to technical applications. By exploiting an elastic snap-through and snap-back instability, we show that the speed of elastomer balloon actuators can be accelerated drastically. This possibility results from the nonmonotonic N-shaped pressure–volume relation of an inflated rubber membrane.[12–14] As soon as the pressure reaches the critical values p_1 or p_2, a further insignificant pressure increase or decrease rapidly changes the membrane volume within milliseconds (Figure 1b). Pressure-controlled deformation is required for the occurrence of an instability,[15,16] therefore the rubber membrane is mounted on a pressure vessel of suitable size. The pressure signal triggering the balloon instability can be provided by any kind of controllable pressure source like a pneumatic compressor, a loudspeaker, or a coupled dielectric elastomer actuator (DEA; Figure 1b). We chose an electroactive acrylic elastomer (3M VHB 4910F) as actuator material to electrically manipulate the pressure of the system.[17,18] VHB has been widely employed due to its large stretchability and high electric breakdown strength.[16] With voltage-triggered balloon instability there is no need for fast and complex pneumatic pressure equipment, after initially pressurizing the chamber. Actuators based on soft balloons are compliant, robust, light weight, simple in structure, and have low costs. Considering these desirable features, they are widely used, ranging from pneumatic applications in medical and health-care robotics to wave-handling systems to transport delicate objects in industry.[19–21] All the mentioned examples would benefit from the increased response speed. To demonstrate the underlying potential, we present prototypes utilizing the snap-through instability of a balloon. In Figure 1c, a fast sorting device is shown, which can be used to sort out defective parts on a conveyor belt. A gripper as depicted in Figure 1d, is fast enough to reliably catch falling objects of various shapes. More controllable gripping can be provided by an appropriate geometric design. A simple example is shown in Figure 1e, where a mounted rod blocks the balloon, resulting in better compliance to the object's shape and thus ensures safe handling.

Except for lab demonstrations, DEAs solely based on VHB acrylic adhesives—favored for achieving giant static strain—have very limited potential for commercial applications that require fast actuation due to viscoelasticity.[22] We overcome this problem by pneumatically coupling two balloon actuators of dissimilar materials. In our approach, a VHB DEA triggers the instability of an inflated natural rubber membrane, which serves as high-speed balloon actuator. Therefore, we are able to report giant deformations within 20 ms. The properties of natural rubber enable high-speed volume expansion rates up to 2300 cm^3 s^{-1} (2600 cm^2 s^{-1} area expansion rate) at forward and backward actuation at frequencies up to 8 Hz. We ensure safe operation, as there is no high voltage at the high-speed balloon actuator. At the same time, the trigger actuator (TA) undergoes small deformations only, averting failure mechanisms such as electromechanical instability or electrical breakdown (EB).[23] The actuation is remote, potentially allowing significant spatial separation into a passive and an electrically active part, which can be arranged "behind the scenes." Subsequent experiments and theory demonstrate how the rubber balloon achieves high-speed and giant deformation by harnessing the snap-through

and snap-back instability. The analysis is based on an electromechanical model using hyperelasticity of elastomer membranes.

2. Results and Discussion

2.1. Experimental Setup and Operation Principle

We build our system of coupled balloons by mounting a dielectric elastomer membrane (VHB) as TA and a rubber balloon featuring low viscoelasticity as high-speed actuator (HSA) on a chamber of suitable volume. In a previous experiment with VHB elastomers, the snap-through occurred on a time scale of 100 s, mainly due to the large viscoelasticity of the VHB elastomer.[15] Thus, VHB is not suitable for fast snap-through. Natural rubber, on the other hand, has comparatively smaller viscoelasticity, enabling large volume changes over a short time. **Figure 2**a compares the "creep-through" of the VHB membrane with a fast snap-through of the rubber membrane. The TA is constantly connected to a high voltage supply providing the voltage signal Φ_{TA} (Figure 2b). The schematic in Figure 2b shows the cyclic process in the pressure–volume plane of the HSA (p-V_{HSA}). Each pressure–volume state of the HSA corresponds to a voltage Φ_{TA} applied to the coupled TA. The operation of the HSA is separated into the following steps: The initial pressure of the system is set to p_A of state A, slightly above the verge of instability of the rubber balloon in state E to enable electrically triggered, giant deformation. Then the voltage Φ_{TA} is applied to the TA membrane. It becomes thinner, volume V_{TA} increases, and the common pressure in the systems falls, consequently decreasing the volume V_{HSA} of the HSA. As soon as the pressure in the system falls below p_B, the HSA snaps back from state B to C. At state D, the voltage Φ_{TA} and volume V_{TA} reach their maximum and V_{HSA} its minimum. Subsequent reduction of the voltage at the TA leads the system to the verge of instability in state E at pressure p_E. The instability is triggered and the HSA snaps through to state F and finally returns to state A when the voltage at the TA reaches its minimum. The unstable states B and E are characterized by the pressure–volume curve of the HSA being tangent to the pressure–volume curve of the air in the whole system.[15] This is the first demonstration of harnessing an electrically triggered snap-*back* instability of a balloon actuator—a key element to achieve fast *cyclic* actuation.

2.2. Discussion of Measured Data

In our experiment, we measured the voltage Φ_{TA} and current I_{TA} of the TA as well as the system overpressure p and determined the volumes V_{HSA} and V_{TA} of the TA and HSA for several cycles of operation. Despite the first two consecutive measurements being noticeably different, the behavior became reproducible after three to four cycles. Figure 2c–f illustrates the measurement data for two consecutive cycles.

By applying sinusoidal voltage (@ 0.5 Hz and 4 kV peak-to-peak) to the compliant electrodes, the TA deforms cyclically (Figure 2c,d and Video S3, Supporting Information). Similar to a pumping piston, the alternating pressure caused by the TA membrane triggers the snap-through and snap-back instability
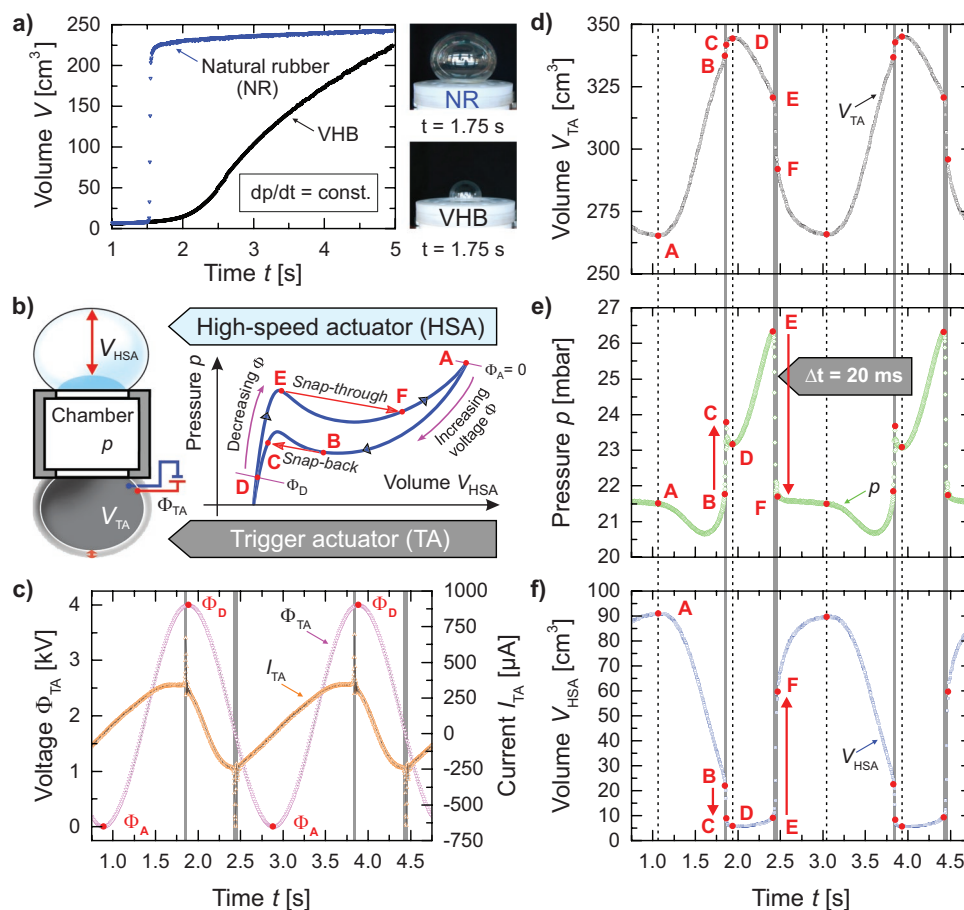
Figure 2. a) Comparison of the volume expansion rate when using elastomer membranes of low viscosity (natural rubber) and high viscosity (acrylic elastomer VHB 3M), while undergoing pressure-controlled mechanical balloon snap-through instability (Video S2, Supporting Information). b) Setup of a HSA remotely triggered by a coupled DEA balloon (TA) and schematic representation of a complete actuation cycle of the HSA in the pressure–volume plane. Giant volume changes occur rapidly as the HSA undergoes snap-back (state B to C) or snap-through (state E to F) instability. c) Sinusoidal voltage applied to the TA is used to trigger instability of a coupled balloon actuator. d) The volume change of an electrically driven DEA balloon actuator (TA) modulates e) the system pressure, f) enabling the coupled HSA to undergo instability with large volume changes.

of the HSA (Figure 2e,f and Video S3, Supporting Information). A suitable prestretch of the TA is necessary to obtain sufficient actuation,[24] required to reach the unstable states B and E of the HSA. We observe that the sudden changes of volume and pressure during the instabilities from state B to C, or from state E to F result in distinct spikes in the current characteristics I_{TA} (orange triangles with black connecting lines in Figure 2c). They originate from the rapid alteration of the capacitance of the electroactive membrane due to the variation in geometry (area and thickness) during inflation or deflation. The observed small currents during operation permit the usage of cheap commercially available low power DC to HV converters for high voltage supply. The time t_{EF} for the HSA to change from state E with volume $V_{HSA,E} = 13$ cm^3 to state F with $V_{HSA,F} = 59$ cm^3 is 20 ms. This results in a high volume expansion rate of 2300 cm^3 s^{-1} (2600 cm^2 s^{-1} area expansion rate in spherical membrane approximation). The total volume change of one half-cycle between state A at volume $V_{HSA,A} = 88.4$ cm^3 and state D with $V_{HSA,D} = 5.9$ cm^3 is about 1398%. The snap-through from state E to F results in a significant pressure drop and a rapid volume increase. During a snap-back instability from state B to state C, the pressure

rises rapidly and the volume drops quickly. The size of these jumps can be modified by changing the volume of the connecting chamber.[15,16] For subsequent theoretical analysis, the measured cyclic time-dependent data sets are plotted parametrically in the pressure–volume plane for the HSA, as well as the voltage applied on the TA versus the volume of the HSA (**Figure 3**).

2.3. Theoretical Analysis

The resulting blue pressure curve in Figure 3a shows the typical hysteretic behavior of elastomer balloons.[25] This hysteresis is due to stretch-induced crystallization (SIC) and viscoelastic effects. Its theoretical analysis is possible within the frame of microscopic theories[26,27] and quasi-linear viscoelasticity,[28] but is not instructive for our purposes. The hysteresis in the pressure–volume plane of the HSA does not change the qualitative picture, though it does influence the exact numbers. We account for this effect by using different shear modulus μ_{HSA} and J_{lim} for the inflation and deflation stages (Table S1 and Figure S1a, Supporting Information).
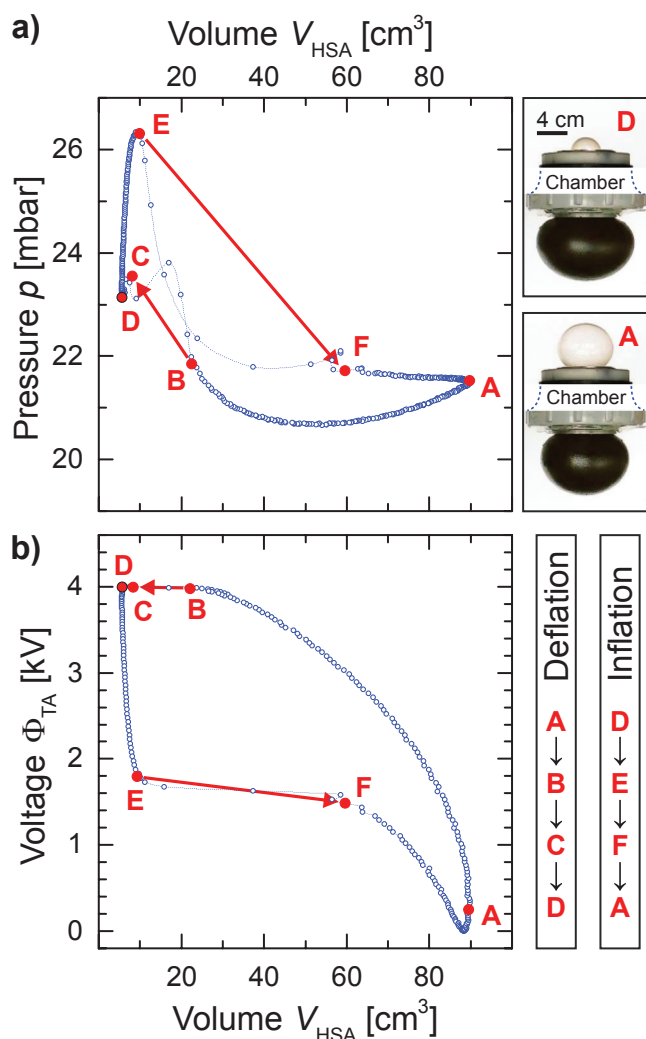
Figure 3. a) Measured pressure and volume data of the cyclic experiment. The system is pressurized to an initial pressure p_A. As voltage is applied to the TA, the change of volume and pressure forces the coupled HSA to undergo the snap-through and snap-back instability (indicated by arrows). The characteristic states A to F of a full actuation cycle correspond to the points marked in Figure 2b. The shapes of the balloon at state A and D of the TA and HSA are depicted for comparison. b) Measured voltage Φ_{TA} applied on the TA plotted as a function of the volume V_{HSA} of the HSA.

For theoretical analysis, the system is idealized by assuming the HSA and TA to be spherical with initial (unstretched) radii R_{HSA} and R_{TA} and thicknesses H_{HSA} and H_{TA}. The membranes of both balloons are taken to be incompressible and thin. When the pressure inside each balloon exceeds the atmospheric pressure p_{atm} by p, the balloons deform to radii $r_{HSA} = \lambda_{HSA} R_{HSA}$ and $r_{TA} = \lambda_{TA} R_{TA}$, where λ are the respective homogenous radial (lateral) stretches. In addition to pressure, the TA is subjected to the voltage Φ_{TA}. We consider quasi-static equilibrium with respect to pressure and voltage. We assume that air is an ideal gas obeying the ideal gas law

$$(p + p_{atm})\left(\frac{4}{3}\pi R_{TA}^3 \lambda_{TA}^3 + \frac{4}{3}\pi R_{HSA}^3 \lambda_{HSA}^3 + V_C\right) = N k_B T \quad (1)$$

here, V_C is the chamber volume, N is the number of air molecules, and $k_B T$ is the temperature in energy units. The amount of air N enclosed by both balloons and chamber is fixed after the valve is closed. The deformation is assumed to be isothermal. In practice, the fast expansion and contraction of the considered prototype actuators may be closer to adiabatic processes, leading to additional effects, which will be discussed elsewhere. The adiabatic relative temperature changes, and the concomitant changes in the shear modulus $\Delta\mu/\mu = \Delta T/T$ can be estimated to be less than 1%. Such minor variations are below the accuracy of the current modeling.

We account for the stiffening of the elastomer at large deformation by using a hyperelastic Gent material model[29] for the elasticity of both balloons, such that the volumetric strain energy density for equi-biaxial deformation (configurational part of Helmholtz free energy) is of the form

$$W_{stretch}(\lambda) = -\frac{\mu J_{lim}}{2}\ln\left(1 - \frac{2\lambda^2 + \lambda^{-4} - 3}{J_{lim}}\right) \quad (2)$$

here, μ is the small-strain shear modulus and J_{lim} is a constant related to the stiffening of the elastomer at large deformation.[29,30] For the dielectric elastomer balloon, we adopt the model of ideal dielectric elastomers,[31] such that the free energy density is the sum of two parts: the elastic energy due to stretching in Equation (2) and the electrostatic energy density due to the polarization of the elastomer, $W_{ele} = D^2/(2\varepsilon)$, where D is the electric displacement and ε is the absolute permittivity.

For any variation of the system, the free energy of each balloon membrane varies by its respective $4\pi R^2 H \delta W$. When the charge on the electrodes of the TA varies by δQ, the applied voltage does work $\Phi_{TA} \delta Q$. When the radius of either balloon varies by δr, the pressure does work $4\pi r^2 p \delta r$. For the HSA, a state of equilibrium is reached when the variation of the free energy of the membrane equals to the work done by the pressure; in the case of the TA, the equilibrium state is reached, when the variation of the free energy of the membrane is equal to the combined work done by the pressure and the voltage. This results in standard N-shaped single-balloon pressure–volume dependences $p_{HSA}(V_{HSA})$ and $p_{TA}(V_{TA}, \Phi_{TA})$, as detailed in the Supporting Information (Equation (S2)). They correspond to the equilibrium conditions of the kinematic set of equations derived previously.[32] Fitting of the pressure–volume data for the rubber (HSA) and VHB (TA) membranes (Figure S1, Supporting Information) results in the values (Table S1, Supporting Information) used in the calculations. They comply with the data reported and used in literature.[16] The relative permittivity ε_r of VHB is taken as 4.7.[33]

The cyclic dynamic behavior shown in Figure 3a,b is modeled in **Figure 4**a,b, with the same notations for the key points. The solid blue curve and the dashed pink curve in Figure 4a do not depend on the TA and visualize the $p_{HSA}(V_{HSA})$ dependences. They correspond to the inflation (solid blue) and deflation (dashed pink) stage—deflation has a smaller μ_{HSA} and J_{lim} value. The *snapping* hysteresis exists also with constant parameters, but the numbers differ significantly. The different black curves combine the $p_{TA}(V_{TA}, \Phi_{TA})$ dependence with Equation (1), and do not depend on the HSA (see Equation (S5) in the Supporting Information for details). They correspond to
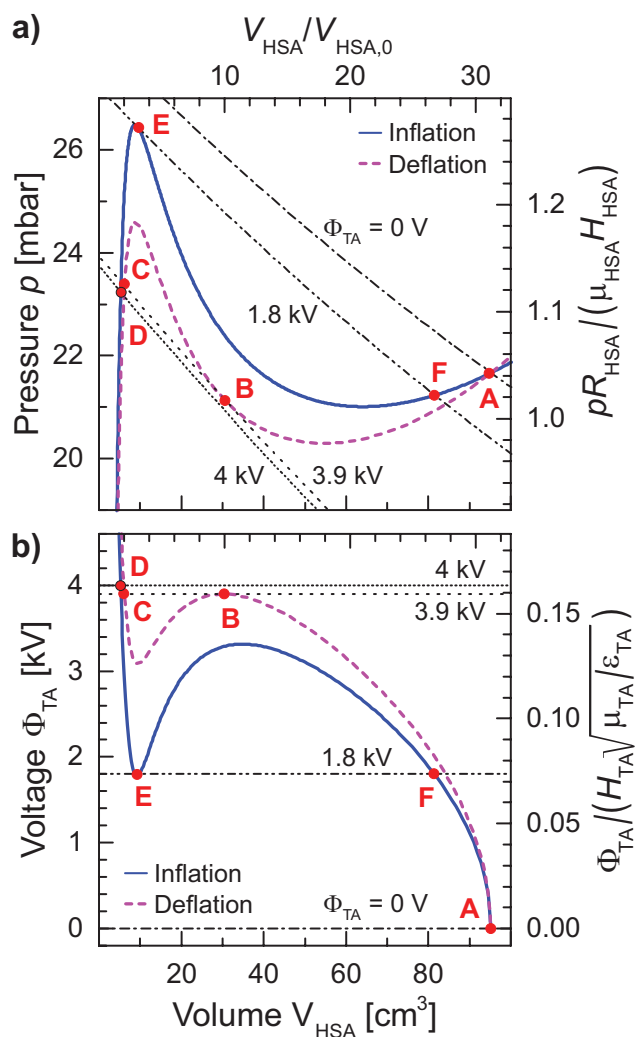
Figure 4. Theoretical a) static pressure p and b) voltage Φ_{TA} applied to the TA membrane as a function of the volume V_{HSA} of the HSA with dimensional left-bottom axes, and dimensionless right-top scales (with inflation μ_{HSA} value). The solid blue and the dashed pink curves represent the inflation and deflation stages and account for the material hysteresis observed in the experiment. Different dotted black curves combine $p_{TA}(V_{TA})$ dependences with air conservation (Equation (1)) for different voltages Φ_{TA}, applied to the coupled TA: 0 V, the snap-through, the snap-back, and the maximum value (see Equation (S5), Supporting Information). The equilibrium pressure–volume states of the HSA for these voltages are marked by red dots and correspond to states indicated in Figures 2 and 3. Parameters are listed in Table S1 in the Supporting Information.

0 V, snap-through, snap-back, and the maximum value of the voltage. The parameters of the system are chosen such that the TA is always strongly stretched, and the applied voltage modulates its pressure. The equilibrium states are the intersections of the blue—or pink—and black curves. Snapping happens, when some of the common solutions disappear, i.e., when these curves become tangential. The snapping path roughly follows (dynamically modified) HSA single-balloon curves. The $p_{HSA}(V_{HSA})$ dependence dictates a large pressure drop with a large volume expansion during snap-through instability, and a smaller pressure rise with a smaller volume

contraction during a snap-back. The snapping magnitude is governed by the HSA properties, for snap-through

$$\Delta p \leq \left(C \frac{\mu H}{R} \right)_{HSA} \text{ and } \frac{V_{HSA,after}}{V_{HSA,before}} \geq \frac{\lambda_{lim}^3}{7^{1/2} \times 3^{3/2}} \text{ (see Equations (S8)–(S10)}$$

and S14, Supporting Information). Here, C is a constant $C \approx 12 \times 7^{-7/6} - 3^{3/2} \lambda_{lim}^{-1} \approx 0.23$ containing the reciprocal of λ_{lim} which is the maximal possible (equal-biaxial) stretch of the HSA according to the Gent model $2\lambda_{lim}^2 \approx J_{lim}$. Without the effects of SIC, the hysteresis in the pressure–volume plane of the HSA vanishes and the blue and pink curves merge, but clearly, the *voltage-induced snapping* hysteresis still persists, though the required voltage difference is significantly lower. Theoretical Figure 4b explains the dynamic voltage behavior, observed in the experimental Figure 3b; it is plotted according to the parametric procedure described in the Supporting Information. The voltages required for snapping depend on the HSA and

TA properties and are of the order of $\Phi_{TA} \approx \left(\frac{HR}{2\varepsilon\lambda_{lim}} \right)_{TA}^{1/2} \left(C \frac{\mu H}{R} \right)_{HSA}^{1/2}$

(Equations (S14) and (S15), Supporting Information). The voltages only weakly depend on the shear modulus of the VHB, μ_{TA}, because the change in the elastic pressure of the HSA between the snapping points is compensated largely by the changes in the electrostatic pressure of the strongly stretched TA. The theoretical predictions of Figure 4 are in a *semi-quantitative* agreement with the experimental results from Figure 3. The details of the theoretical analysis and the influence of various parameters are described in depth in the Supporting Information.

With this good agreement between our model and our experiment, an optimized system that maximizes actuation performance can be designed in the future.

3. Conclusion

Inspired by nature, we introduced an actuator, which harnesses a snap-through and snap-back instability for giant high-speed deformations. By using a system of coupled balloons, remote, high-voltage triggered, bistable actuation is possible. Consisting of an electrically active and passive part, this actuator can be operated in a safe regime, far away from the EB voltage of the dielectric elastomer. Its combination of fast volume change rate and large maximum deformation makes this concept an attractive candidate for use in soft robotics.

4. Experimental Section

Membrane Material and Preparation: The membrane of the HSA was made of high-quality natural rubber Durex Ultra with a diameter of 32 mm and a thickness of 50 µm without prestretch. High-quality rubber improved the reliability and speed of the snap-through instability. The DE material used for the TA was the acrylic elastomer 3M VHB 4910F with a diameter of 45 mm and prestretch $\lambda_{pre} = 1.8$, coated on both sides with compliant electrodes. A stretchable electrode was prepared by coating the DE membrane with carbon grease (MG chemicals 846-80G diluted with ELBESIL B50 silicon oil).[34] The membrane geometries and mounting holes for the screws to fixate the membranes were cut out using a laser cutter (Trotec Speedy300).

Fabrication of the Setup: Both membranes were mounted on a cylindrical chamber with a volume of $V_C = 7$ dm^3 and clamped with rigid rings. A valve for the supply with pressurized air and the pressure sensor was directly connected to the chamber.

Measurement Equipment: System-pressure p was measured by a Jumo p30 pressure sensor and the volumes V_{TA} and V_{HSA} of both membranes were obtained by video analysis and contour detection using the image processing library National Instruments IMAQ. The DEA was connected to a Trek Model 610D high-voltage power supply combined with a function generator (Hewlett Packard 33120A) to achieve a sinusoidal waveform. A DAQ-card (National Instruments PCI-6281) was used for data acquisition.

Supporting Information

Supporting Information is available from the Wiley Online Library or from the author.

Acknowledgements

Conflict of Interest

The authors declare no conflict of interest.

Keywords

[1] R. F. Shepherd, A. A. Stokes, J. Freake, J. Barber, P. W. Snyder, A. D. Mazzeo, L. Cademartiri, S. A. Morin, G. M. Whitesides, *Angew. Chem., Int. Ed.* **2013**, *52*, 2892.

[2] M. Raibert, K. Blankespoor, G. Nelson, R. Playter, *IFAC Proc. Vol.* **2008**, *41*, 10822.

[3] R. F. Shepherd, F. Ilievski, W. Choi, S. A. Morin, A. A. Stokes, A. D. Mazzeo, X. Chen, M. Wang, G. M. Whitesides, *Proc. Natl. Acad. Sci. USA* **2011**, *108*, 20400.

[4] E. Brown, N. Rodenberg, J. Amend, A. Mozeika, E. Steltz, M. R. Zakin, H. Lipson, H. M. Jaeger, *Proc. Natl. Acad. Sci. USA* **2010**, *107*, 18809.

[5] J.-Y. Nagase, N. Saga, T. Satoh, K. Suzumori, *J. Intell. Mater. Syst. Struct.* **2012**, *23*, 345.

[6] N. Kellaris, V. G. Venkata, G. M. Smith, S. Mitchell, C. Keplinger, *Sci. Rob.* **2018**, *3*, eaar3276.

[7] M. L. Smith, G. M. Yanega, A. Ruina, *J. Theor. Biol.* **2011**, *282*, 41.

[8] P. T. Martone, M. Boller, I. Burgert, J. Dumais, J. Edwards, K. Mach, N. Rowe, M. Rueggeberg, R. Seidel, T. Speck, *Integr. Comp. Biol.* **2010**, *50*, 888.

[9] Y. Forterre, J. M. Skotheim, J. Dumais, L. Mahadevan, *Nature* **2005**, *433*, 421.

[10] A. Pal, D. Goswami, R. V. Martinez, *Adv. Funct. Mater.* **2019**, *30*, 1906603.

[11] Y. Forterre, P. Marmottant, C. Quilliet, X. Noblin, *Europhys. News* **2016**, *47*, 27.

[12] I. Müller, P. Strehlow, *Rubber and Rubber Balloons: Paradigms of Thermodynamics*, Springer, Berlin, Germany **2004**.

[13] R. W. Ogden, *Proc. R. Soc. A* **1972**, *326*, 565.

[14] M. F. Beatty, *Appl. Mech. Rev.* **1987**, *40*, 1699.

[15] C. Keplinger, T. Li, R. Baumgartner, Z. Suo, S. Bauer, *Soft Matter* **2012**, *8*, 285.

[16] T. Li, C. Keplinger, R. Baumgartner, S. Bauer, W. Yang, Z. Suo, *J. Mech. Phys. Solids* **2013**, *61*, 611.

[17] S. Rudykh, K. Bhattacharya, G. deBotton, *Int. J. Non-Linear Mech.* **2012**, *47*, 206.

[18] F. Carpi, G. Frediani, D. De Rossi, *IEEE/ASME Trans. Mechatronics* **2010**, *15*, 308.

[19] C.-H. King, M. O. Culjat, M. L. Franco, J. W. Bisley, E. Dutson, W. S. Grundfest, *IEEE Trans. Biomed. Eng.* **2008**, *55*, 2593.

[20] T. Wang, J. Zhang, J. Hong, M. Y. Wang, *Soft Rob.* **2017**, *4*, 61.

[21] A. De Acutis, L. Calabrese, A. Bau, V. Tincani, N. M. Pugno, A. Bicchi, D. E. De Rossi, *Smart Mater. Struct.* **2018**, *27*, 074005.

[22] S. Rosset, P. Gebbers, B. M. O'Brien, H. R. Shea, *Proc. SPIE* **2012**, *8340*, 834004.

[23] J.-S. Plante, S. Dubowsky, *Int. J. Solids Struct.* **2006**, *43*, 7727.

[24] S. J. A. Koh, T. Li, J. Zhou, X. Zhao, W. Hong, J. Zhu, Z. Suo, *J. Polym. Sci., Part B: Polym. Phys.* **2011**, *49*, 504.

[25] D. R. Merritt, F. Weinhaus, *Am. J. Phys.* **1978**, *46*, 976.

[26] V. N. Khiem, M. Itskov, *J. Mech. Phys. Solids* **2018**, *116*, 350.

[27] A. Gros, E. Verron, B. Huneau, *J. Mech. Phys. Solids* **2019**, *125*, 255.

[28] R. De Pascalis, W. J. Parnell, I. D. Abrahams, T. Shearer, D. M. Daly, D. Grundy, *Proc. R. Soc. A* **2018**, *474*, 20180102.

[29] A. Gent, *Rubber Chem. Technol.* **1996**, *69*, 59.

[30] A. Cohen, *Rheol. Acta* **1991**, *30*, 270.

[31] Z. Suo, *Acta Mech. Solida Sin.* **2010**, *23*, 549.

[32] J. Zhu, S. Cai, Z. Suo, *Polym. Int.* **2010**, *59*, 378.

[33] G. Kofod, P. Sommer-Larsen, R. D. Kornbluh, R. Pelrine, *J. Intell. Mater. Syst. Struct.* **2003**, *14*, 787.

[34] S. Rosset, H. R. Shea, *Appl. Phys. A* **2013**, *110*, 281.

1903391 (7 of 7)

Supporting Information

A Lesson from Plants: High-Speed Soft Robotic Actuators

Richard Baumgartner, Alexander Kogler, Josef M. Stadlbauer, Choon Chiang Foo, Rainer Kaltseis, Melanie Baumgartner, Guoyong Mao, Christoph Keplinger, Soo Jin Adrian Koh, Nikita Arnold, Zhigang Suo, Martin Kaltenbrunner,* and Siegfried Bauer

Supporting Information

A Lesson from Plants: High-Speed Soft Robotic Actuators

Richard Baumgartner, Alexander Kogler, Josef M. Stadlbauer, Choon Chiang Foo, Rainer Kaltseis, Melanie Baumgartner, Guoyong Mao, Christoph Keplinger, Soo Jin Adrian Koh, Nikita Arnold, Zhigang Suo, Martin Kaltenbrunner, and Siegfried Bauer*

HSA and TA balloons with connecting chamber

The HSA and TA balloons, together with the connecting chamber C, contain a *constant* amount of gas molecules N, which obey the ideal gas law:

$$(p_{atm} + p)(V_{HSA} + V_{TA} + V_C) = NkT \tag{S1}$$

Here, the corresponding volumes V are labeled by subscripts. Assuming *isothermal* sealed equilibrium conditions, both sides of this equality remain *constant*.

The equilibrium *over*pressure p inside the *thin spherical* balloon made of an *incompressible elastomer* can be expressed as follows:[12,35-37]

$$
\begin{aligned}
p &\overset{1}{=} \frac{H}{R}\frac{W_{str,\lambda}}{\lambda^2} \overset{2}{=} \frac{H}{R}W_{str,J}\underset{J_\lambda/\lambda^2}{4(\lambda^{-1}-\lambda^{-7})} \overset{3}{=} \frac{H}{R}\frac{2\mu(\lambda^{-1}-\lambda^{-7})}{1-(2\lambda^2+\lambda^{-4}-3)/J_{lim}}\ \text{a} \\
p &\overset{4}{=} \frac{H}{R}\frac{(W_{str,\lambda}-W_{ele,\lambda})}{\lambda^2} \overset{5}{=} \frac{H}{R}\frac{2\mu(\lambda^{-1}-\lambda^{-7})}{1-(2\lambda^2+\lambda^{-4}-3)/J_{lim}} - \frac{2\varepsilon\Phi^2\lambda}{RH} \overset{6}{=} p_{str}+p_{ele}
\end{aligned}
\tag{S2}
$$

Here, H and R are the thickness and the radius of an unstretched balloon, λ is the *radial* stretch, W_{str} is the *configurational* part of the volumetric energy density and $W_{str,\lambda}$ denotes its derivative with respect to λ. The expression $S2_1$ (labeled by 1 over the equality in Equation S2) represents the most general form, where W_{str} is expressed in terms of a single stretch variable λ assuming incompressibility and equal-biaxial stretch conditions. The equality $S2_2$ assumes that W_{str} depends only on the 1st stretch invariant J, which implies (under the same conditions):

$$W_{str} = W_{str}(J), \quad J = \sum_{i=1}^{3} \lambda_i^2 - 3 = 2\lambda^2 + \lambda^{-4} - 3, \quad J_\lambda = 4(\lambda - \lambda^{-5}) \tag{S3}$$

J_λ denotes the derivative of the 1st stretch invariant J with respect to λ. Finally, the equality S2$_3$ is based on the (isothermal) Gent model (Equation 2, Main Text) with shear modulus μ and limiting stretch invariant value J_{lim}. For this model, the energy derivative with respect to the invariant J has the simple form: $W_{str,J} = \dfrac{\mu/2}{1 - J/J_{\text{lim}}}$. More complex material models should use the representation S2$_1$. Formulas S2$_{1-3}$ apply to the HSA balloon, for which the electrostatic energy does not have to be taken into account. Equation S2$_3$ can be used to estimate the stored energy in the HSA by calculating the integral under the $p_{HSA}(V_{HSA})$ curve in Figure 3a or 4a. The stored energy can also be determined by using the elastic energy density in Equation 2 with an elastomer volume of $V_{el} = (4\pi R^2 H)_{HSA} \approx 0.05\,\text{cm}^3$ (values from Table S1). Both methods yield the same result for the energy density of 4 J/cm^3 and an energy of 0.2 J for the maximum extension in state A (Figure 4a).

The pressure p in the TA balloon obeys similar mathematical expressions, when the contribution of the electrostatic energy W_{ele} is considered together with W_{str}. In SI units, the electrostatic energy density is:

$$W_{ele} = \frac{\varepsilon E^2}{2} = \frac{\varepsilon \Phi^2}{2h^2} = \frac{\varepsilon \Phi^2 \lambda^4}{2H^2} \tag{S4}$$

Here, ε is the *full* dimensional dielectric constant that includes vacuum permittivity ε_0. The last equality implies $h = H/\lambda^2$ due to incompressibility. When the TA actuator is kept at a *constant voltage*, the work done by the battery *reverses the sign* of the electrostatic contribution.[31,38] This results in the expressions S2$_{4-5}$ for the pressure where W_{ele} enters with a negative sign. In the expression S2$_6$ we subdivide the overpressure p in the TA into stretching and (negative) electrostatic contributions, which we use later.

Equation S1 and S2 are *similar* to the *equilibrium* conditions discussed in the references.[15,16,32,39] However, these papers describe only one balloon (with or without a connecting chamber), some employ Neo-Hookean or Mooney-Rivlin material models, concentrate on the deviations from the spherical shape (studied numerically), influence of the pre-stretch, *dynamic* behavior, etc.

Quasi-static equilibrium analysis

Equation S1 and S2$_{3,5}$ (for the Gent models of the HSA and the TA) provide three equations for three unknown variables: p, λ_{HSA} and λ_{TA}. All coefficients are constant, while the voltage Φ_{TA} is varied quasi-statically. Parameters used in the calculations are listed in Table S1. The material properties μ and $J_{\lim}$ can be measured independently for both elastomers, and are assumed to be known, as well as the relative dielectric constant ε_r. The same holds for the volume of the connecting chamber V_C, the external pressure p_{atm}, the temperature T, and the unstretched balloon thicknesses H. The unstretched radii R (or corresponding volumes $V_0 = 4\pi R^3/3$) are inferred from the inflation/deflation experiments with a single balloon (see Figure S1, and the discussion after the Equation S8 and S9). In practice, R is an *equivalent spherical radius*, which is varied within physically admissible range for fitting. The amount of gas N is found from the *experimental* product on the left side of Equation S1. This product is constant within 0.3% everywhere during the cycle, which justifies our modelling approach.

It is instructive to analyze the behavior of the system in the plane of HSA volume and common pressure. The Equation S2$_{1\text{ or }3}$ defines a standard N-shaped single-balloon curve $p_{HSA}(V_{HSA})$.[12-14,35-37] This curve is shown as a solid blue line in Figure 4a. A similar dashed pink curve has smaller values of μ_{HSA} and $J_{\lim}$, to account for the inflation-deflation hysteresis in the material properties.

Equation S2$_{4 \text{ or } 5}$ defines an N-shaped curve $p_{TA}(V_{TA}, \Phi_{TA})$, which depends also on the applied voltage Φ_{TA}. To present p_{TA} as a function of V_{HSA}, we find the latter from the conservation law in Equation S1 by substitution. This yields a parametric (V_{HSA}, p) curve, with V_{TA} as a parameter along the curve:

$$(V_{HSA}, p) = \left(\frac{NkT}{p_{atm} + p_{TA}(V_{TA}, \Phi_{TA})} - V_C - V_{TA}, p_{TA}(V_{TA}, \Phi_{TA}) \right) \tag{S5}$$

These curves are shown in Figure 4a and S2a for several voltages Φ_{TA}, using differently dotted black lines. The resulting curve on the right side of Equation S5 depends only on the properties of the TA balloon. We did not use the $p_{HSA}(V_{HSA})$ dependence at all. Thus, the black curves are independent of the blue—or pink—curve, which facilitates analysis and fitting. Their qualitative behavior can be understood as follows. For the used parameters, V_C is constant and the term $NkT / (p_{atm} + p_{TA})$ varies much less than V_{TA}. As a result, the dependence $p_{TA}(V_{TA}) \approx p_{TA}(const - V_{HSA})$ reveals a *mirrored* N-shaped behavior in the (V_{HSA}, p)-plane, depicted in Figure S2b over a larger pressure and volume scale. One can see, that this argumentation is *not exact* but very helpful for a deeper understanding.

The equilibrium of the system corresponds to the intersection of the blue—or pink—and black curves and moves along the former with changing voltage. The values of the voltages chosen for plotting in Figure 4a and S2a correspond to 0 V, snap-through, snap-back, and the maximum voltage. Snapping happens, when some of the common solutions disappear, i.e., when the blue—or pink—and the black curves become tangential to each other. The black curves indicate where the snapping *ends*, but the snapping path roughly follows the single HSA balloon curves (modified by dynamic effects). If the volume of the connecting chamber satisfies the condition $V_C \gg V_{HSA} + V_{TA}$, the snap-through and snap-back curves are almost horizontal, with $p \approx const$. Larger voltages Φ_{TA} are required in this case.

The general analysis can be performed as follows: Substitute $p(\lambda_{HSA})$ from Equation S2$_3$ into the conservation law (Equation S1), and resolve it with respect to $V_{TA} \leftrightarrow \lambda_{TA}$. This gives the $\lambda_{TA}(\lambda_{HSA})$ dependence. Substitute $p(\lambda_{TA}, \Phi_{TA})$ from Equation S2$_5$ into the conservation law and resolve it with respect to $V_{HSA} \leftrightarrow \lambda_{HSA}$. This yields the $\lambda_{HSA}(\lambda_{TA}, \Phi_{TA})$ dependence. With this construction, $\lambda_{TA}(\lambda_{HSA})$ does not depend on TA *material* parameters, and $\lambda_{HSA}(\lambda_{TA}, \Phi_{TA})$ does not depend on HSA material values. The intersection of these two dependences in the $(\lambda_{HSA}, \lambda_{TA})$-plane for different values of the voltage Φ_{TA} defines the equilibrium of the system, and all variables can be expressed parametrically via either λ_{HSA} or λ_{TA}. The corresponding curves in the $(\lambda_{HSA}, \lambda_{TA})$ and (V_{HSA}, V_{TA})- planes are shown in Figure S3a and S3b.

The voltage Φ_{TA} is derived from the Equation S2$_5$, using the relation for the overpressure $p_{str}(\lambda_{TA})$ defined in Equation S2$_6$:

$$\frac{2\varepsilon_{TA}\Phi_{TA}^2\lambda_{TA}}{R_{TA}H_{TA}} = p_{str}(\lambda_{TA}) - p \tag{S6}$$

From here, using p a $p(\lambda_{HSA})$, and λ_{TA} a $\lambda_{TA}(\lambda_{HSA})$, as defined above, the equilibrium voltage can be expressed as a composite function of λ_{HSA}:

$$\Phi_{TA}(\lambda_{HSA}) = \sqrt{\frac{R_{TA}H_{TA}}{2\varepsilon_{TA}\lambda_{TA}(\lambda_{HSA})}(p_{str}[\lambda_{TA}(\lambda_{HSA})] - p(\lambda_{HSA}))} \tag{S7}$$

Equation S7 is used together with $V_{HSA} = V_{HSA,0}\lambda_{HSA}^3$ for the parametric dependence $(V_{HSA}, \Phi_{TA}) = (V_{HSA,0}\lambda_{HSA}^3, \Phi_{TA}(\lambda_{HSA}))$ shown in Figure 4b by the blue and pink curves. Dotted black lines correspond to the constant voltage of 0 V, snap-through, snap-back, and the maximum value.

Parameter estimation

The following observations elucidate the influence of different parameters on the system behavior. All parameters are listed in Table S1. The snap-through and snap-back happen near the maximal and minimal pressures of the $p_{HSA}(V_{HSA})$ curve. The *maximum* can be found in Neo-Hookean approximation:

$$p \overset{1}{\approx} \frac{\mu H}{R} 2(\lambda^{-1} - \lambda^{-7})$$

$$\lambda_{max} \overset{2}{\approx} 7^{1/6} \approx 1.38, \qquad V_{max} \overset{3}{\approx} 7^{1/2} V_0 \approx 2.65 V_0, \quad p_{max} \overset{4}{\approx} 12 \times 7^{-7/6} \mu H / R \approx 1.24 \mu H / R \qquad (S8)$$

The *minimum* can be found keeping the leading powers of $\lambda \gg 1$, because the next terms typically differ by a factor of λ^{-6}. For the Gent model in Equation S2$_3$, one can (numerically) recalculate $J_{lim}, \lambda_{lim}, V_{lim}$ into each other using the relations $J_{lim} = 2\lambda_{lim}^2 + \lambda_{lim}^{-4} - 3$, $V_{lim} = V_0 \lambda_{lim}^3$. This correspondence is listed in Table S2 (inflation data), and we can interchange these parameters at will. Good accuracy is provided by the following expressions.

$$p \overset{1}{\approx} \frac{\mu H}{R} \frac{2\lambda^{-1}}{1 - (2\lambda^2 - 3)/(2\lambda_{lim}^2 - 3)}$$

$$\lambda_{min} \overset{2}{\approx} \frac{\lambda_{lim}}{\sqrt{3}} \approx 2.77, \qquad V_{min} \overset{3}{\approx} \frac{\lambda_{lim}^3}{3^{3/2}} V_0 = \frac{V_{lim}}{3^{3/2}} \approx 21.2 V_0 = 0.19 V_{lim}, \qquad (S9)$$

$$p_{min} \overset{4}{\approx} 3^{3/2}(1 - 3\lambda_{lim}^{-2}/2)\lambda_{lim}^{-1} \frac{\mu H}{R} \approx 1.01 \frac{\mu H}{R}$$

The numerical values use the HSA data from Table S2. The Equations S8 and S9 are helpful for the fitting of the experimental data and the verification of material properties. The following ratios are useful:

$$\frac{V_{min}}{V_{max}} \approx \frac{\lambda_{lim}^3}{7^{1/2} 3^{3/2}} \approx 8.02, \qquad \frac{p_{max}}{p_{min}} \approx \frac{12 \times 7^{-7/6}}{3^{3/2}(1 - 3\lambda_{lim}^{-2}/2)\lambda_{lim}^{-1}} \approx 1.22 \qquad (S10)$$

The volume V_{max} yields the estimate for V_0 and R. The volume ratio V_{min}/V_{max} estimates the maximal stretch λ_{lim} in Gent model. The pressure ratio p_{max}/p_{min} provides a consistency

check for the material parameters, while $p_{\max}$ estimates the combination $\mu H / R$. If H is known, μ can be adjusted using this estimation and vice versa.

Figure S1a shows the fitting of the pressure-volume data for a *single* rubber HSA balloon with pronounced inflation/deflation hysteresis. This hysteresis is mainly due to the stretch-induced crystallization (SIC)[26,27,40] and viscoelasticity.[28] We do not discuss these effects here, but account for them phenomenologically, by using a smaller shear modulus μ_{HSA} and $J_{\lim}$ for the deflation stage, due to a higher crystalline fraction there. SIC softens the material with respect to the *overall* stretch, and shortens the chains in the *amorphous* fraction, as seen in the experimental hysteresis curves.[26,27,40] The μ_{HSA} value for deflation is slightly lower than in Figure 4, due to minor setup differences, such as a slightly larger maximal HSA extension (at which it was held for seconds), and 30 times slower pneumatic cycling in Figure S1a. These factors soften the elastomer and are reflected in a smaller μ_{HSA} value.

Figure S1b shows the fitting of the pressure-volume data for a *single* VHB TA balloon with compliant electrodes, but without applied voltage. As the TA balloon operates in a narrow interval of stretches and volumes, the inflation/deflation discrepancy is not crucial here. However, VHB is highly viscoelastic on a slow timescale preventing fast snap-through or snap-back.[15,16] VHB parameters change with time and the number of cycles. The first cycles differed significantly due to Mullins and Payne effect. After the 3rd cycle, which is fitted in Figure S1b, the differences became much less pronounced. The conditions for a single TA slightly deviated from the coupled case: No voltage on the TA, much slower pneumatic cycling, full stretching and relaxation cycle, as opposed to permanent high stretch with only moderate variations (shown in Figure 2d) and a shorter overall duration of the experiment. All these factors reduced long-term viscoelastic yielding, resulting in somewhat larger values for H and μ for the single TA membrane, which remained in the physically admissible range (see

Table S1). Fitting of the coupled system with these, or even larger R, H, μ values for the TA produced too flat snapping pressure behavior, and overly large HSA volumes as a result.

The Gent model provides a reasonable fit for the TA within its range of operation (200–400 cm^3). It is less suited for large VHB stretches, which are viscoelastic and rate dependent (right side of the blue and red curves in Figure S1b—rupture occurs at a volume of 1303.5 cm^3). The viscoelasticity of the TA also delays its elastic response to the applied voltage (as can be deduced from Figure 2c and 2f), leading to moderate discrepancies between theory and experiment, which can be seen near the maximum extension (zero voltage) point A in Figure 3b and 4b.

Approximation for the highly stretched TA

The parameters of the system are such that the TA remains highly stretched, with λ close to $\lambda_{\lim} \gg 1$. Its volume V is close to $V_{\lim}$, and does not change much. In this situation, one can further simplify the approximation given by Equation S9$_1$, and express it in terms of volume V:

$$\frac{2\lambda^{-1}}{1-(2\lambda^2-3)/(2\lambda_{\lim}^2-3)} \approx \frac{1}{\lambda_{\lim}-\lambda} \approx \frac{3\lambda_{\lim}^{-1}V_{\lim}}{V_{\lim}-V} \tag{S11}$$

This gives the leading terms for the pressure of TA in Equation S2$_5$:

$$p_{TA} \approx \left(\frac{\mu H}{R} \frac{3\lambda_{\lim}^{-1}V_{\lim}}{V_{\lim}-V} - \frac{2\varepsilon\Phi^2\lambda_{\lim}}{RH} \right)_{TA} \tag{S12}$$

This result depends on $V_{\lim}$ rather than on V_0 (although both are related) and the difference of V and $V_{\lim}$. A value for $V_{\lim}$ can be deduced from the logarithmic derivative of Equation S12 for $\Phi = 0$, which results in:

$$V_{\lim} = \frac{\Delta(pV)}{\Delta p} \tag{S13}$$

V_{lim} can be estimated from Equation S13, using two or several adjacent experimental data points. The same expression holds with V a λ, but λ is not directly measured in the experiments.

Influence of the voltage

To understand the influence of the voltage, we note that snap-through occurs near the $(V_{\text{max}}, p_{\text{max}})$ values of the HSA balloon, see Equation S8$_{3,4}$, and snap-back near $(V_{\text{min}}, p_{\text{min}})$ given by Equation S9$_{3,4}$. In the lowest-order approximation for a very large connecting chamber the volume of the TA does not change significantly, and the black curves in Figure 4a become almost horizontal. Then, the change in the *elastic* HSA pressure between the snapping points should be matched by the *changes* in the *electrostatic* pressure in the strongly stretched TA:

$$p_{\text{max}} - p_{\text{min}} \approx \left(C \frac{\mu H}{R} \right)_{HSA} \approx \left(\frac{2\varepsilon\lambda_{\text{lim}}}{HR} \right)_{TA} (\Phi^2_{TA,back} - \Phi^2_{TA,through})$$

$$C \approx 12 \times 7^{-7/6} - 3^{3/2}(1 - 3\lambda_{\text{lim}}^{-2}/2)\lambda_{\text{lim}}^{-1} \approx 0.23$$

(S14)

This relation elucidates main *trends* in the system parameter dependences. However, it cannot be used for *quantitative* predictions, because for the current setup, the slope of the black curves is significant, and the snap-back deviates substantially from the $(V_{\text{min}}, p_{\text{min}})$ point (Fig. 4a). The situation is further complicated by the SIC hysteresis in the HSA and viscoelastic effects in the TA.

In optimal operating conditions the snap-through occurs at minimal voltage, $\Phi_{through} \approx 0$. p_{max} of the HSA should be matched by the pressure of the strongly stretched TA. This helps to choose its parameters, such as thickness H, or pre-stretch (i.e., effective R and V_0). Then, the minimal possible snap-back voltage can be estimated from the Equation S14.

$$\Phi_{\substack{back \\ minimal}} \approx \left(\frac{HR}{2\varepsilon\lambda_{lim}} \right)^{1/2}_{TA} \left(C\frac{\mu H}{R} \right)^{1/2}_{HSA} \tag{S15}$$

For our numbers this gives 2.4 [kV] using inflation values (2.58 [kV] accounting for inflation/deflation hysteresis), which lies in the realistic range. Used conditions are not far from optimal, because $\Phi^2_{through}[kV] \approx 1.8^2_{3.24} = 3.9^2_{15.21} \approx \Phi^2_{back}$. The volume range of actuation can be only moderately increased without drawbacks. A significantly larger actuation magnitude requires bigger actuators, which can be readily designed using the guidelines described in the Equation S8, S9, S14 and S15.

Estimation of the force for sorting applications

The force acting on the drinking cup in Figure 1c can be deduced from the Video S1 (see Supporting Video). After the contact with the high-speed actuator the cup's velocity is about 1.8 m/s. For a cup of 5 g, this corresponds to a momentum of about 9 x 10-3 kg m/s. With a contact time of 36 ms (9 frames of the high-speed video at 250 fps) this suggests a (normal) force of 0.25 N acting on the cup. The (maximal) gripping force depends on the particular sorting geometry and can be estimated from the overpressure in the HSA, which is around 25 mbar (Figure 3). Considering the current setup, contact areas of up to 40 cm^2 are feasible, providing a (normal) force around 10 N. Even when assuming a rather low friction coefficient of 0.1, objects of 100 g mass can be readily handled. Such forces can be easily tolerated by a human. The punch of the actuator was tested by bare hand and does not present any hazard in operation.

References

[35]   K. Volokh, *Mechanics of soft materials*, Springer, New York, USA **2016**, p. 155.

[36]   A. F. Bower, *Applied mechanics of solids*, CRC Press, Boca Raton, USA **2010**, p. 794.

[37]   G. A. Holzapfel, *Nonlinear solid mechanics*, Wiley, Chichester, USA **2000**, p 455.

[38]   C. Keplinger, M. Kaltenbrunner, N. Arnold, S. Bauer*, Proc. Natl. Acad. Sci.* **2010**, *107*, 4505.

[39]   E. M. Mockensturm, N. Goulbourne, *Int. J. Non. Lin. Mech.* **2006**, *41*, 388.

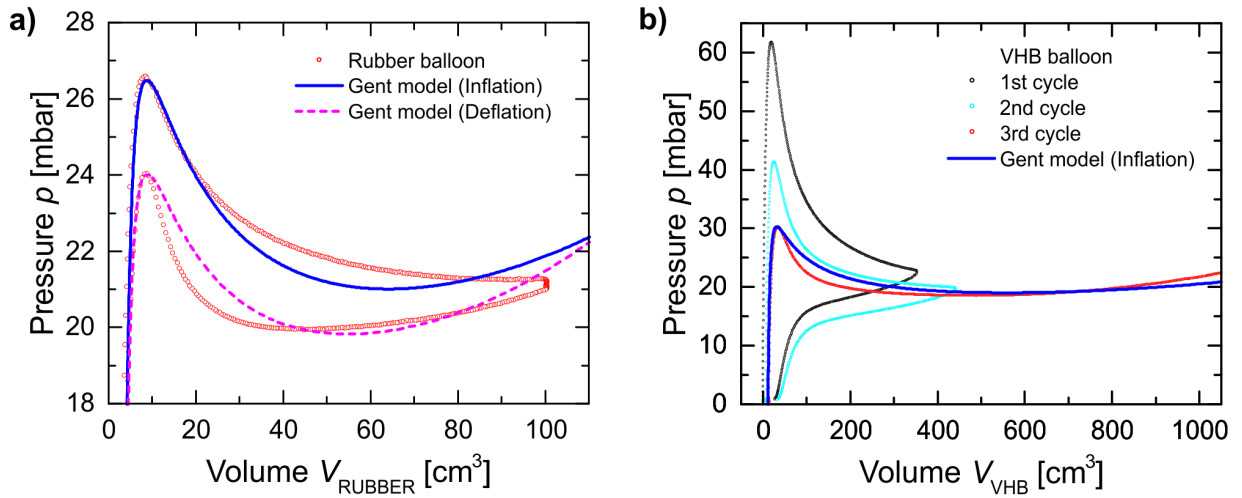[40]   A. Gros, B. Huneau, E. Verron, M. Tosaka, *J. Mech. Phys. Solids* **2019**, *125*, 164.

Figure S1. a) Fitting of the pressure-volume data of the inflation and deflation of the rubber membrane (HSA alone) using the Gent model. b) Inflation of the VHB balloon (TA alone). The 3rd cycle is fitted, the modulus in the cycling experiments is lower due to accumulated viscoelastic effects. All parameters are listed in Table S1.
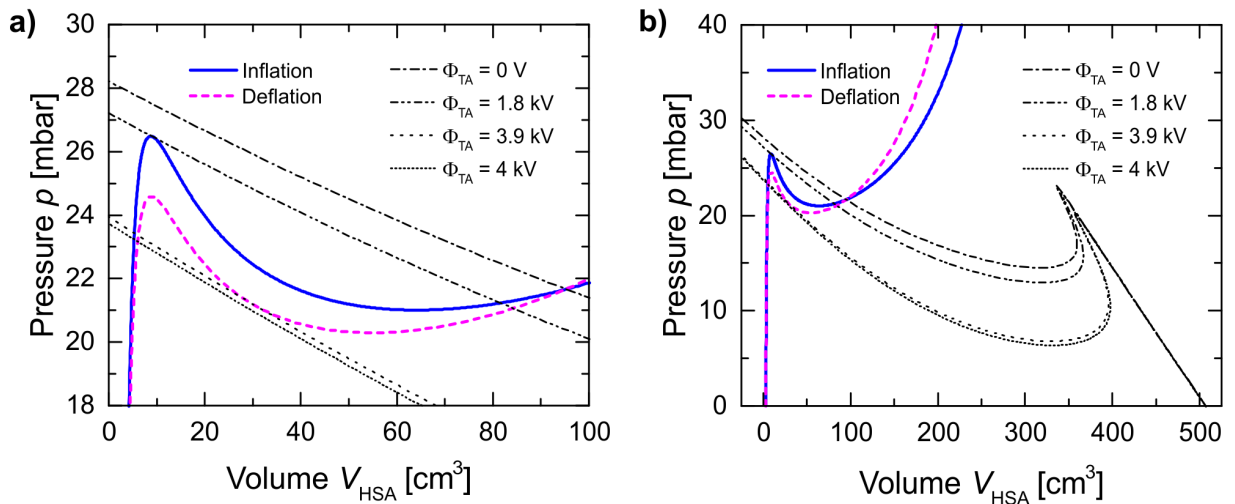

Figure S2. a) The Figure 4a from the main text is reproduced here in simplified form for convenience. b) The same dependence as in (a), over a wider range of volumes and pressures. The black dotted curves are based on the single-balloon $p_{TA}(V_{TA})$ dependence combined with the conservation law (Equation S1), and demonstrate a *mirrored* N-shaped dependence. The system operates in the range of large stretches λ_{TA}.
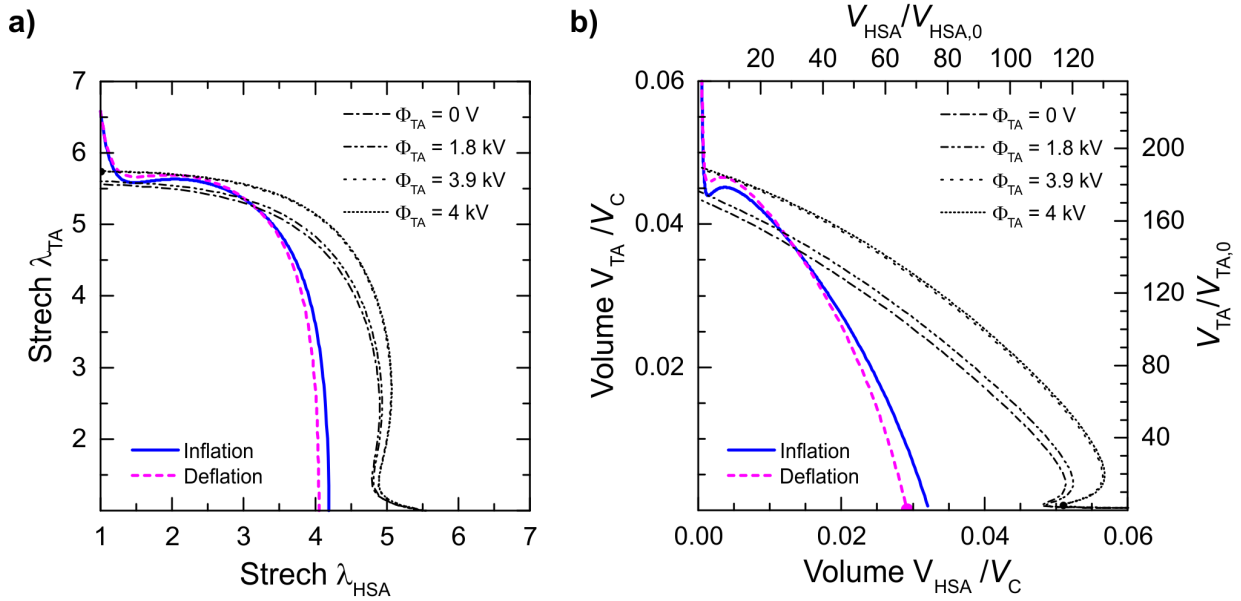
a)

b)

Figure S3. a) Interrelation between the stretches, which follows from the ideal gas law (Equation S1). Solid blue and dashed pink curves $\lambda_{TA}(\lambda_{HSA})$ are obtained using the substitution of $p(\lambda_{HSA})$. Dotted black curves $\lambda_{HSA}(\lambda_{TA},\Phi_{TA})$ are obtained using the substitution of $p(\lambda_{TA},\Phi_{TA})$. All parameters are the same as in Figure 4 or S2. b) Dependences from Figure S3a (recalculated into the balloon volumes) normalized to the volume of the connecting chamber. A slightly different range of stretches is shown, to make the volume scales the same for both axes.

Table S1. Parameters used in the calculations

| Balloon actuators	μ [kPa]	J_{lim}	H [cm]	R [cm]	V_0 [cm³]	ε_r
Coupled TA	16	77	0.086	0.75	1.77	4.7
TA alone [a]	33.7	77	0.1	1.4	11.5	
Coupled HSA (infl.; defl.) [b]	374; 346	43; 38.5	50×10^{-4}	0.9	3.05	
HSA alone (infl.; defl.) [a,b]	374; 338	43; 38.5	50×10^{-4}	0.9	3.05	
Common parameters	p_{atm} [kPa]	NkT [J]	T [K]	N [mole]	V_C [cm³]	
	101.325	760.8	293.15	0.312	7000	

[a] Experiment with only a single balloon of the corresponding material; [b] Different values for inflation and deflation account for the material hysteresis

**Table S2.** Secondary calculation parameters

Balloon actuators	λ_{lim}	R_{lim} [cm]	V_{lim} [cm^3]	$\Phi_{through}$ [kV]	Φ_{back} [kV]
TA	6.32	4.74	447.1	1.8 (1.825) [a]	3.9 (3.975) [a]
HSA [b]	4.8	4.32	336.8		

[a] Experimental; [b] Inflation parameters are used

Supplementary Videos
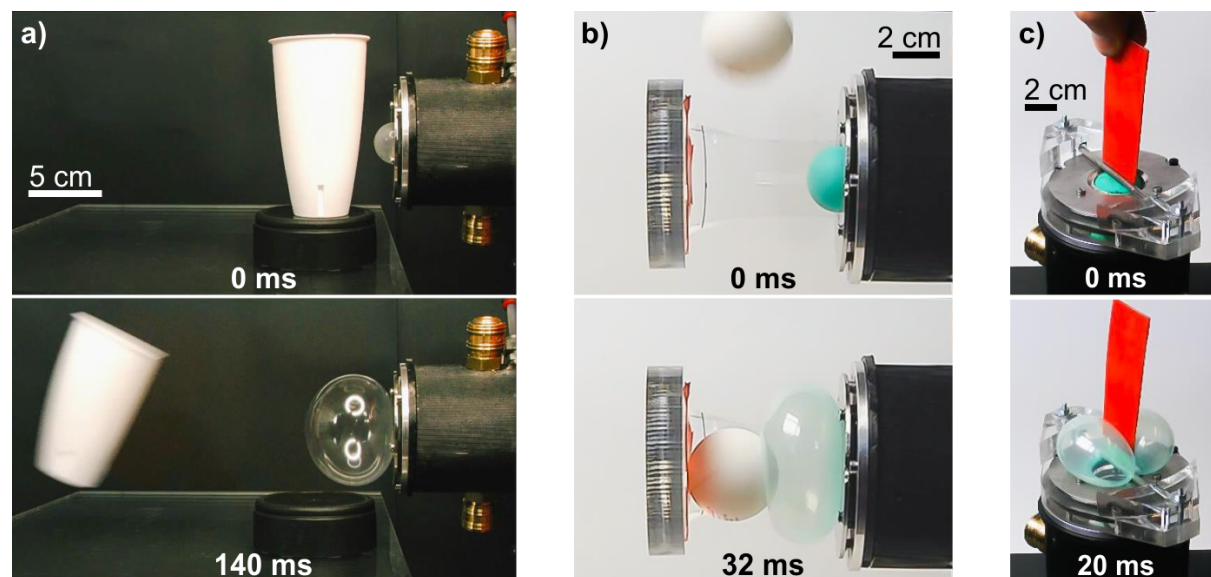
Video S1. Snapshots from the Video *'Prototypes utilizing snap-through instability'* demonstrating possible applications in real-time and slow-motion: (a) *'snap-sorting'*, (b) *'snap-catching'* and (c) *'snap-gripping'*.
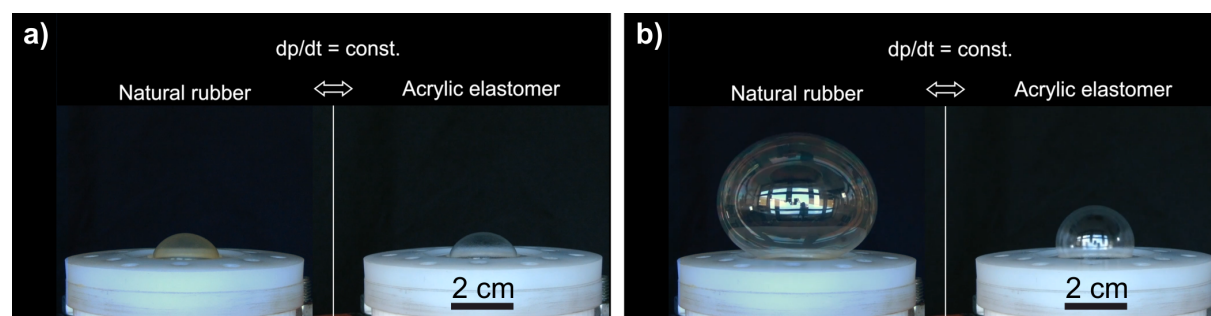
Video S2. Still images of the Video *'Comparison of natural rubber and the acrylic elastomer VHB'* showing the temporal response.
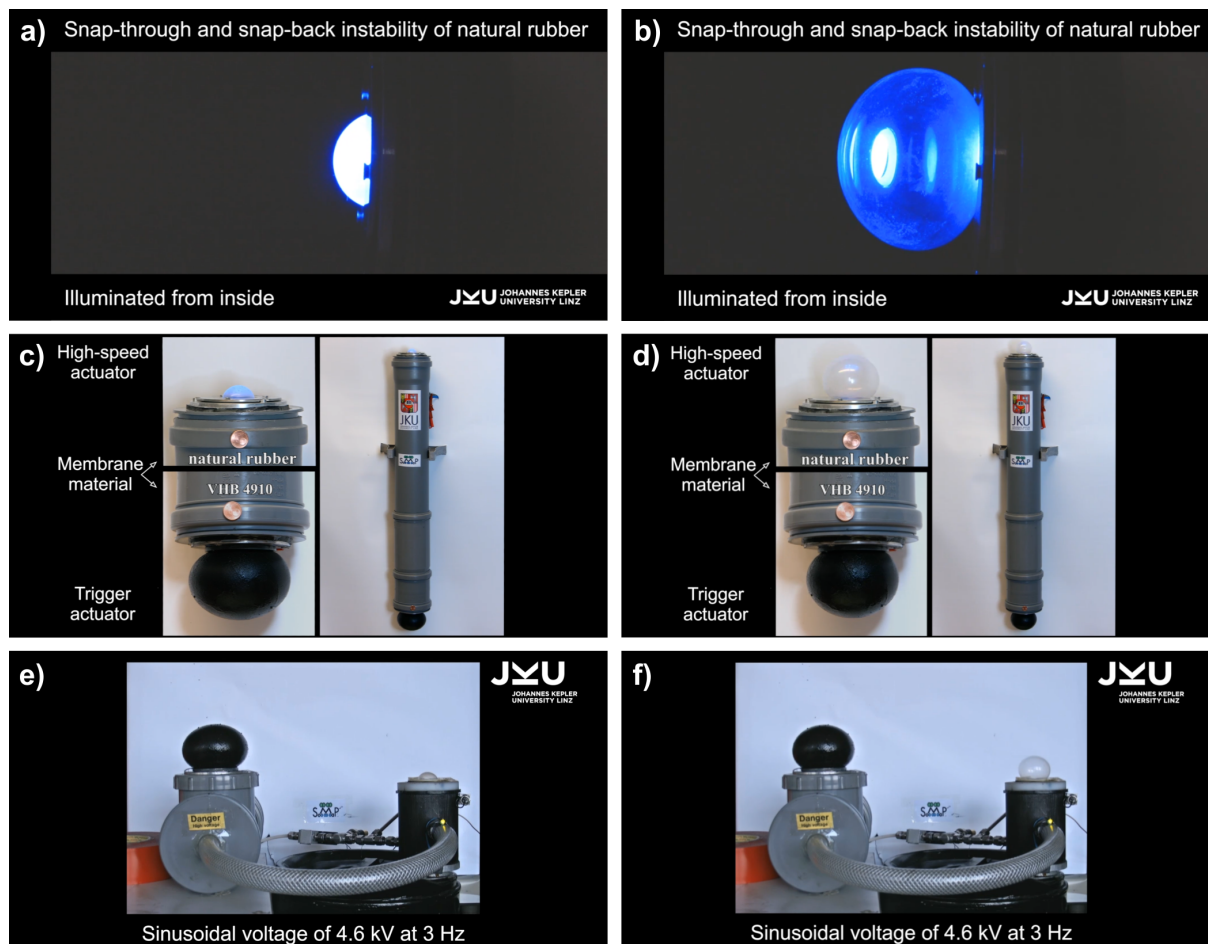
Video S3. Still images of the Video *'High-speed voltage-triggered soft actuator harnessing instability'* illustrating the fast response due to the snap-through and snap-back instability of natural rubber in (a) and (b), the principal set-up in (c) and (d), as well as the cyclic deformation by applying sinusoidal voltage (4 kV at several frequencies) to the trigger actuator in (d) and (f).